



OTC 8269A

## Numerical Test Tanks: Computer Simulation/Test Verification of Major Ocean Engineering Problems for the Off-Shore Oil Industry

C. R. Orloff/FMC Corporate Technology Center and M. Krafft/FMC SOFEC

Copyright 1997, Offshore Technology Conference

This paper was prepared for presentation at the 1997 Offshore Technology Conference held in Houston, Texas, 5-8 May 1997.

This paper was selected for presentation by the OTC Program Committee following review of information contained in an abstract submitted by the author(s). Contents of the paper, as presented, have not been reviewed by the Offshore Technology Conference and are subject to correction by the author(s). The material, as presented, does not necessarily reflect any position of the Offshore Technology Conference or its officers. Electronic reproduction, distribution, or storage of any part of this paper for commercial purposes without the written consent of the Offshore Technology Conference is prohibited. Permission to reproduce in print is restricted to an abstract of not more than 300 words; illustrations may not be copied. The abstract must contain conspicuous acknowledgment of where and by whom the paper was presented.

### Abstract

With the increase in knowledge in computer-based numerical simulation methods and the advent of high-speed computers, complex ocean engineering flow and wave-structure impact problems can now be performed to predict transient free surface impact wave shapes as well as forces and moments on full-size structures and moored ships. Numerical results, in combination with selected test tank measurements for verification purposes, form the basis of the concept of the Numerical Test Tank (NTT). Some sample approximate solutions illustrating the application of Computational Fluid Dynamics (CFD) methods to solution of practical ocean engineering problems are presented to illustrate the methodology involved and then compared to model test tank results at moderate ocean depths. The numerical method produces reasonable agreement with Froude-scaled transient test tank free surface wave shapes during hull-large wave impact as well as test force and pressure histories at key model measurement stations. Although some differences arise in the validation comparisons due to details of the numerical simulation set-up (cell size distribution, convergence criteria, turbulence model, boundary conditions, etc.) the use of Froude Number scaling for model wave impact results is at least qualitatively demonstrated from the present results.

Specifically, full three-dimensional, transient, viscous Navier-Stokes numerical solutions are made for a large amplitude Stokes' wave train impacting on a full-scale, pitching FPSO hull (Green Water Problem) and compared to some MARIN model test tank results at moderate scaled ocean depths. The numerical method produces qualitative agreement with Froude-scaled test basin transient on-deck

surface wave shapes during wave-hull impact as well as force and pressure histories at key model measurement stations. This comparison thus provides qualitative verification of the use of Froude number scaling to a good degree of approximation for forces, wave shapes and pressures during (Green Water) wave-hull impact.

Additionally, CFD methods have been used to compute selected current-derived force and moment coefficients similar to those presented in the 1994 OCIMF publication "Prediction of Wind and Current Loads on VLCC's". Selected force coefficients are numerically computed for a stationary, scale model and a full size standard vessel hull and compared to model test-measured force coefficient values. Preliminary limited calculated results show good agreement with OCIMF coefficients but clearly indicate that further numerical investigations are to be made to account for depth, current magnitude, hull orientation, viscous and turbulence effects on full size hulls to verify simple Froude number scaling laws.

The apparent utility of the Numerical Test Tank approach, as illustrated by the preliminary verification examples presented, indicates that the computational approach holds promise for improving detailed knowledge of design loads for offshore structures and moored ships subject to wave and current loading.

### Introduction

Prediction of transient pressure and load conditions resulting from Green Water wave interaction with FPSO hull and deck structures has traditionally been determined by scale model tests in large model basin facilities. Froude number scaling is often used to scale model test loads, time, wave shapes and pressures from shallow depth test basin measurements to predict loads and wave shapes experienced by full-size hulls at water depths varying from shallow to deep. Several difficulties and unknown factors arise from this procedure, however, when applied to large wave-hull interaction. These include: differences in wave characteristics from free ocean conditions compared to test-tank, moving-paddle generated wave trains (e.g., distance from the wave maker to model for developed, classical wave forms to occur,

steepness effects) and questions related to the applicability of Froude scaling to wave-hull splashing impact dynamics (as the assumptions underlying gravity wave dominated behavior may not be applicable for localized on-deck, wave-deck structure interaction impact and splashing behavior with air-entrainment occurring during splashing). Further questions arise related to the effects of hull pitching and heave motions on Froude scaling of model to full scale hull loads and wave shapes and finally, further questions related to upstream wave reflection patterns from the impacted hull that condition the incoming wave and alter its pre-impact steepness and shape (and thus subsequent loads and wave shapes on successive impacts). All of these considerations may influence the accuracy of simple application of Froude scaling of test basin results to full-scale hull loads.

In order to resolve the effects of these considerations on the applicability of Froude scaling laws, computer modeling studies were performed utilizing FMC/SOFEC-developed software based upon the FLOW-3D/96 CFD code<sup>1</sup>. The FLOW-3D/96 CFD code is a three-dimensional, finite-difference, structured grid code based upon development of the SOLA-VOF<sup>2,3</sup> method with extensive free-surface capability to solve full viscous Navier-Stokes equations with various turbulence model choices. For the current Green Water problem, a three-dimensional FPSO hull was first modeled from MARIN test model specifications<sup>6,7</sup> using an ANSYS obstacle preprocessor<sup>5</sup> and then transferred to FLOW-3D/96 as a flow obstacle.

The computer-modeled hull (Figure 1) consists of 60,000 tetrahedron elements to ensure a smooth outer hull surface with respect to typical near-hull computational cell sizes originating from the active 600,000 cell three-dimensional computational mesh. The FPSO FLOW-3D/96 obstacle model is next modified by adding a deck superstructure and special source-code modifications that allow prescription of the displacement of the hull rotation axis (CG) from a reference axis and the prescription of the pitching frequency and maximum pitching amplitude at the bow. Additionally, the heave amplitude and heave frequency of the hull can likewise be prescribed. From available MARIN test data<sup>6,7</sup> for the model hull, the test pitch and heave parameters can be input into the computer model for a given wave train interacting with the model hull. To duplicate the test wave train, the FLOW-3D/96 source code was further modified to include a Stokes' wave train with a prescribed wave length, wave speed to depth relationship<sup>8,9</sup> to approximate the wave characteristics of the MARIN test series for the modeled FPSO hull. From MARIN test data from hull-wave dynamic motion, additional prescriptions of the wave-hull pitch and heave phase angles, current velocity and hull draft depth are input into the modified source code approximating (but not exactly matching) the MARIN test tank results at a prescribed test tank depth.

The computational model therefore is set up to duplicate

key parameters of the MARIN model tests with respect to hull pitch and heave characteristics as well as incoming wave train characteristics and current magnitude to a good degree of approximation. Computational grid size has been adjusted locally to allow for expected flow regions experiencing sharp velocity gradients and/or free surface curvature changes over small distances. Additionally, the boundary location of the wave train source is located sufficiently far upstream of the (pitching and heaving) hull obstacle to eliminate reflected wave interactions with the wave source boundary over typical wave-hull interaction times. Absorbent boundaries are used to damp reflected waves at all wave numbers at lateral boundaries to the hull direction.

Two separate FPSO hull computer models are used in the analysis to follow: The first model (M-1) duplicates the MARIN test tank hull model size and geometry; the second model (M-2) is scaled up full-size FPSO dimensions. The first (M-1) model is used to compare MARIN test data (forces and pressures at transducer locations and wave shapes from capacitance wave gages and photographic surveys) to computed results for transient (Green Water) wave-hull impact using test specifications for wave train and hull dynamics. The second full scale (M-2) model (i.e., at full FPSO dimensions) is used for computation of transient wave-hull interaction wave shapes, forces and pressures to gage the effects of geometric scale on forces, pressures and wave shapes on the Froude-scaled test data. Presumably the full-scale FPSO results will (perhaps) indicate some Reynolds Number contributions to alter velocity distributions, forces, pressures and transient wave shapes and thus modify the Froude scaling laws as a result. Since the MARIN M-1 test data have been already Froude-scaled<sup>6,7</sup> to full-scale FPSO results, comparison to M-2 calculated results will reinforce the validity of Froude scaling for Green Water problems.

For purposes of comparison of MARIN test data to the M-1 computational model, the following table is given for the MARIN model testing constraints and key flow parameters compared to the specifications for the FLOW-3D/96 computational analysis.

Model Fixity Model	Table 1	
	MARIN Test	FLOW-3D
	(Scaled to Full Size Hull)	
Surge	No	No
Heave	Yes	No
Pitch	Yes	Yes
Hull Contour Match	Yes	Yes
Input Wave Type	Near-Sinusoidal	Stokes
Rotation About CG	Yes	Yes
Bow Flare	No	No
Freeboard	8.88 m	8.88 m
CG Above Base	14.22 m	14.22 m



CG Forward Midship 6.72 m                      6.72 m

**Flow and Hull Geometric Parameters**

Wave Height	8.42 m	8.0 m
Current	0.0 m/sec	0.1 m/sec
MX. Hull Pitch Rate	-----	~ 0.85 deg/sec
Pitch Frequency	11 Hz	~ 10 Hz
Wave Period	11.0 sec	11.0 sec
Scaled Water Depth	150 m	150 m
Phase Angle	0.0 rad	0.0 rad
Distance from Prow to		
Vertical Bridge	30.0 m	30.0 m
Bulwark	No	No
Hull Length	260.34 m	260.34 m
Beam	47.10 m	47.10 m
Draft	17.52 m	17.52 m
Deck Edges	Sharp	Rounded

MARIN data quoted is based upon best author estimates from transducer output traces, tables and geometric data. Calculations shown exclude surge effects to match test geometry conditions. Several differences between MARIN test input data and computational input data make the comparisons to follow qualitative in nature as the effects of some of these differences on the transient flow development may be significant. In this sense, the verification process still leaves unanswered questions related to the effects of physical as well as computational convergence, stability, finite difference solution scheme and cell size distribution parameter variations on numerical simulation results.

**Results**

Application of ANSYS<sup>5</sup> modeling to produce the FPSO model hull with a vertical deck box housing has been performed and the results shown in **Figure 1**. The forward location of the deck box is positioned so that the front surface conforms to the MARIN test plate position on the scale model. From the wave specifications listed in Table 1, FLOW-3D/96 calculations were performed to predict the transient wave impact sequence at different times within the impact cycle. The hull pitch frequency, wave-hull phase angle and a small current value in the wave direction are specified from Table 1 values to approximate some MARIN test parameters to a good degree of accuracy. No top deck railing or deck obstacles are included in the model beyond the hull-fixed deck box housing shown. Only the front third of the hull is shown in the computer model as this is the region of interest for wave impact studies. The incoming Stokes wave train is initiated at a distance equal to several hull lengths upstream of the bow; this modeling artifice allows for uniformization of the wave packet and establishment of the computer-generated wave particle trajectory-depth relationships to approximate

analytical predictions<sup>8,9</sup>. Results for the three-dimensional Green Water impact wave forms are shown in **Figures 1** through **20**.

A typical wave impact cycle, typically about 12 seconds in duration, is demonstrated by the wave patterns shown in these figures. **Figure 2** shows the initial  $t = 0.0$  sec hull-wave configuration prior to wave impact of the incoming 8.4 m amplitude Stokes wave train. Some water remains on-deck from a previous wave-hull encounter cycle which has left some minor disturbance patterns on the ocean surface. At  $t = 1.0$  sec, the (long wave length) wave front is seen to rise above the deck prior to over-spilling onto the deck. **Figures 3** through **7** indicate the progression of the over-spilling wave onto the deck. A distinct set of three-tiered gravity waves appear (**Figs. 6, 7**) in the over-spillage wave sequence which qualitatively correlate to MARIN test observations (**Figure 25**) over the same time period in the wave development sequence. By  $t = 4.5$  sec, first contact with the vertical deck plate is made (**Fig. 7**) while the over-spillage wave front zone of influence moves radially outward to influence the local shape of the incoming long period waves. Note also that part of the incoming wave flows over the sides of the hull to impact upon the side portions of the deck box structure. As will be shown later, this secondary, delayed side-wall impact results in side pressure and force maximums at the lateral base sections of the deck box structure. By  $t = 6.0$  sec, the deck is completely enveloped (**Fig. 9**) with water with velocities on the order of 2 to 4 m/sec along the deck symmetry plane. A clockwise circulatory flow region appears imbedded at the base of the deck-vertical front plate region near the hull symmetry axis with an approximate height of 0.10 of the local upward water height of the front plate structure. The upward velocity along the vertical plate above the circulatory flow region appears to be on the order of 7 m/sec for times on the order of 9.0 sec into the cycle. **Figures 8** through **12** document the upward rise of the central part of the on-deck flow onto the vertical front plate. The maximum vertical rise height of about 20 m above the deck on the vertical front plate appears to occur at about 9 sec after initial wave encounter with the hull.

The water accumulation on the deck, in combination with the downward pitching hull, then produces a combination of hydrostatic and dynamic pressure that severely loads the foredeck structure. **Figures 10** through **18** document the water unloading from the foredeck. After the maximum vertical water height on the front deck plate is achieved, relaxation of the on-deck water accumulation begins. This unloading occurs by side overflow over the upward pitching deck (**Figures 15** through **18**) accompanied by a transient relaxation gravity wave structure (**Figs. 13, 14**) on the surface of the forward sloping water mass on the deck. The up-pitching hull tends to delay water loss from the deck as the forward moving water encounters an angle change in the deck

(due to changing pitch angle) resulting in a local depth increase as the velocity slows near the prow region. **Figures 15, 16 and 17** indicate that as the hull pitches upward, the water mass on deck shifts backward again altering the overflow patterns and causing a secondary transient force on the deck-mounted vertical plate. **Figures 15 to 20** demonstrate that the net effect of the off-deck flow and pitching hull is to create an outward propagating disturbance trough in the water before the prow section that influences the incoming wave train shape; this effect will therefore influence subsequent wave impact force and pressure distributions to a minor degree depending on the phase and amplitude relationship between the incoming and outgoing wave trains.

For the present application, only a small effect on subsequent wave trains and concomitant pressure and force distributions is noticed. Typical pressure distributions are shown in **Figure 21** ( $t = 10.5$  sec) and **Figure 22** ( $t = 8.5$  sec). For the first  $t = 10.5$  sec. case, large deck hydrostatic loading is experienced in addition to high loading at the box corner-deck interfaces as a large mass of water resides on the deck; for the earlier time ( $t = 8.5$  sec) case, maximum loading occurs near the hull symmetry plane in the region just forward of the vertical plate. The vertical plate does not appear to experience the maximum pressure loading compared to deck loads except for initial impact times ( $6.0 < t < 8.0$  sec). This may be due to the formation of a circulatory region at the base of the front wall which subsequently turns the flow streaklines upward and parallel to the vertical wall. Since the flow is gradually directed upward and somewhat parallel to the front plate after initial impact by the imbedded circulatory zone, wall pressures are lower compared to deck pressures during impact ( $6.0 < t < 9.0$  sec).

Some comparisons to Froude scaled MARIN test data for Table 1 parameters are shown in **Figures 24 and 25**. From **Figure 25**, MARIN measured wave profiles can be qualitatively compared to computed results in **Figures 6 to 8** at similar times in the wave over-spillage regime; here the match to the local multistep gravity wave train shape is evident. For a more quantitative comparison, **Figure 24** shows transient MARIN scaled model transducer-area-integrated force measurement profiles F3 and F4 (vertical plate symmetry axis at the 0.4 and 0.75 plate height locations) and pressure traces P1 and P2 (P1 pressure at 0.125 plate height at 0.4 plate width and P2 pressure at 0.125 plate height on the symmetry axis). The vertical plate is at a scaled distance of about 30 m from the prow while the scaled plate height is 20 m. Geometric scale ratio from model to full size hull is 1:60. Comparison of traces shows reasonable agreement between test and computed values for Table 1 parameters over similar comparison times. MARIN inferred velocity traces<sup>6,7</sup> HV1 and HV2, taken at 0.5 plate height on the symmetry plane and 2.5 m forward of the plate and 5.0 m off from the symmetry plane respectively, can be directly compared to computer results. For HV2, computer results

show a maximum wall velocity of about 7.2 m/sec compared to a peak inferred test value of about 8.0 m/sec. For HV1, test values peak over 20 m/sec while computed values are somewhat less- perhaps due to lack of refinement of the computational grid in a zone of complex, transient high shear flow patterns characteristic of a developing imbedded circulatory flow region at or near the measurement station. In summary, results from the FLOW-3D/96 computational model using the pitching full-size FPSO hull (set at the same phase angle as test conditions) appear to be in reasonable qualitative conformance with the scaled MARIN model test data. Scaled forces and pressures appear to approximate computed results at scaled time with traditional Froude scaling laws<sup>6,7</sup>. Further, the calculated deck flow patterns appear to qualitatively match the observed patterns over complete a wave impact cycle. The presence of subsidiary gravity wave trains appearing on the surface of major on-deck flows [e.g., wave trains on the surface of the initial over-spillage deck flow (**Figures 6, 7, 8**) and on the "piled-up" impact fluid surface (**Figures 11, 12 and 13**) are typical of the relaxation structures associated with steep surface angle water accumulations under varying lateral forces. Pressure distributions indicate that major pressure maximums are confined to the foredeck (**Figure 22**) at early stages of wave inundation before plate impact. Peak pressures then occur at the base of the foredeck and vertical plate intersection during the maximum vertical height phase of wave-plate impact (**Figure 21**) with high pressure on the deck at later times as the upward pitching hull tends to trap water on deck (**Figures 13 to 18**).

For engineering estimates [as the pressure scale is omitted in the (non-color) figures], peak impact deck pressure in the region immediately ahead of the vertical plate appears to be on the order of the hydrostatic pressure at the bottom of the hull while maximum deck pressure appears to be about half this value at earlier and later vertical plate pre-impact times (but spread over a large deck area depending upon the cycle time). The complete set of pressure histories<sup>11</sup> serve to yield the results shown in **Figure 24**. Since Froude scaling applies between model and full-size hull (i.e., for  $L$  the geometric scale factor, time scales as  $L^{1/2}$ , velocity as  $L^{1/2}$ , forces as  $1.025 L^3$ , pressures as  $1.025 L$  and moments as  $1.025 L^4$  and the 1.025 value results from the sea to fresh water density ratio), it appears that the effects of viscosity are negligible in estimating scaled values. As a result, the Green Water transient wave shapes, forces and pressures obtained from the full hull computational model appear to be in reasonable qualitative conformance with some available test data for similar wave train parameters. It is also necessary to point out differences between the numerical simulation results and MARIN test data. The major differences are the amount of water captured on the deck (the simulation shows a greater active amount on-deck than the thin sheet observed colliding with the plate from test photographs<sup>6,7</sup>) and the side flow

impact dynamics (the simulation shows the passing wave to overflow the deck from the side while this is not observed from the tests). These differences may be due to a greater pitch declination used for the simulation compared to the test value. Additional differences may arise from the exclusion of heave in the computer model. Investigations are currently underway to include this effect and gauge the effects on final wave patterns. Although Numerical Test Tank methodology is in early stages of verification and more computational-to-test comparison work remains, qualitative comparisons to date appear to indicate that the NTT method is at least promising as an alternate way to provide structural loading results and tests of scaling law applicability.

### OCIMF Force and Moment Coefficients

As an additional exercise of the Numerical Test Tank procedure, some preliminary results are presented for computer predictions of force coefficients of the MARIN Model 5612 hull. The small scale body plan and the measured current coefficients of this hull are derived from Reference 12. Further computations are compared with the 1994 OCIMF data<sup>10</sup>. The hull shape is again made with an ANSYS 60,000 tetrahedron model from MARIN hull contour specifications (Figure 23). A typical model test lateral force coefficient (CY) plot is shown in Figure 26 for different (deep) water depth (WD) to draft (T) ratios and current angle-to-center-plane-of-the-hull symmetry axis angle of attack (positive angle away from the zero degree stern position). The procedure used is to choose a typical current velocity (usually in the range of 1.0 m/sec) for the calculation of the X, Y force components on the full size hull given a prescribed angle of attack, water depth and draft ratio.

For the present application, a uniform velocity profile is prescribed. By next dividing the calculated force components by  $\frac{1}{2} \times (\text{sea water density}) \times (\text{current velocity})^2 \times (\text{projected side view hull area})$ , the CX (along the hull symmetry axis) and CY (normal to the hull symmetry axis) coefficients are determined. Forces arise from a combination of pressure and viscous shear resistance effects on the hull. Various curves are shown in the OCIMF/94 report for 40% loaded draft (ballasted) and 100% loaded draft tankers as well as for different bow shape configurations. Some preliminary calculations and comparison curves shown in Figure 26 refer to sample calculations for a conventional bow, fully loaded tanker for WD/T ratios between 1.05 (shallow water) to >6.0 (deep water).

Results obtained from sample FLOW-3D/96 calculations are plotted in Figure 26 only for sample deep water cases. The continuative boundary conditions available from the FLOW-3D/96 code at the exit planes are such that starting transient wave reflections from the hull will occur both from the initiation of a current past a stationary obstacle (hull) as well as periodic wake shedding interacting with an exit

boundary. Therefore sufficient damping must be introduced from viscosity and turbulence models to absorb some wave energy. Additionally, energy absorbent boundaries in the form of inclined porous ramps and/or sink obstacles are useful for the purpose of obtaining steady-state solutions in compact computational domains after low-amplitude, low energy transient surface waves are damped (or absorbed) after long computational times. These considerations apply when the three-dimensional computational domain size is limited by economic factors. For cases for which this domain can be on the order of several million cells, then wave reflection problems can be mitigated as the waves can be propagated outward from the hull and never meet a reflective boundary before steady-state conditions are established. Since the former condition applies, given the current limitations in practical computational run times, the several artifices mentioned above are necessary to help obtain flow solutions in reasonable computational times (usually >>200 cpu-hrs on Pentium Pro systems).

The solution points shown in Figure 26, which include internal and boundary damping mechanisms and 1500 hour real time simulations, will have some unavoidable low amplitude, low frequency oscillations in CX and CY and moment coefficient values; therefore, statistics must be employed to obtain a best estimate mean value with a standard deviation (Fig. 26). For the present comparisons, only preliminary 90 degree calculations are shown for  $3.0 < WD/T < 16.0$  ratios to test the deep water OCIMF values; later comparisons await further calculations for different parameter sets. Calculated points and error bands indicate approximate agreement with OCIMF data for the deep water cases calculated. Point 1 (Figure 26) corresponds to  $WD/T = 4.4$ , point 3 to  $WD/T = 7.83$ , point 4 to  $WD/T = 9.38$  and point 6 to  $WD/T = 16.0$ . It is of interest to note that quadrupling the WD/T ratio does not lead to significant changes in the CY coefficient provided deep water conditions ( $WD/T > 6$ ) hold. Values shown are calculated based upon a 22.3 m draft compared to 18.5 m scaled test value; therefore, calculated values may be a bit higher than standardized values (although ideally the WD/T ratio is the only key scaling parameter). Ideally, if sufficient computational cells are available, then a critical cell size exists below which force and moment predictions remain constant. Exploration of this effect is complicated by the large number of key parameters that determine stable numerical solutions.

For the Green Water problem, Froude scaling is apparently adequate as an approximate scaling factor due to the apparent lack of importance of viscous, turbulence and splashing effects acting on the separated wave over-spilling the deck. The scaling approximation result considerably simplifies the transfer of model to full scale hull results for the scaled depth given. Investigation of the scaling law applicability at different depths is currently under



investigation pending further available test results. For the OCIMF coefficients, the test model and computer model are the same size so that viscous, pressure and wave drag effects are modeled equally for both test and computer model. The adequacy of the current computer simulation is shown for deep water WD/T values but indication is given that more refinement in flow stability criteria related to cell size criteria (and other key geometric and physical parameters) is necessary together with development in wave damping boundary conditions to ensure high accuracy solutions in limited computational domains. Results shown are therefore to be regarded as preliminary.

### Summary

The NTT method is currently in an early stage of development awaiting further theoretical and numerical solution development techniques (as well as extensive test corroboration) before it becomes a standard tool for off-shore wave structure interaction load prediction. Since the potential to provide direct transient load prediction by computational means without the reliance upon scaling parameters is a result of NTT methods, the furtherance of computational methods is clearly beneficial to the improvement of load prediction methods vital to design of off-shore structures. The results of this paper then provide a first step toward this goal and hopefully encourage further development of the technology toward practical application in the design of off-shore structures under unsteady and steady state wave and current loading.

From the two sample analyses presented, conformance to available test data appears to indicate the utility of the computational approach to provide a supplemental information source to scale model testing. In many cases, three-dimensional computational results provide insight into details of the flow field not usually available from tests due to the technical limitations of traditional test probes and the limited number of placements available in a flow field; in this sense, solutions for pressure, velocity, turbulent intensity, etc., are available at all computational nodes rather than select probe sites.

Provided test verification work is continued to explore the refinement of computational models and techniques, the Numerical Test Tank (NTT) method can increase in application for off-shore wave-structure loading problems to ultimately provide an additional source of transient load distribution information. A further feature of the NTT method is the resolution of the effects of appropriate scale parameters to correlate model tests to full-size hull results. For complex fluid-structure interactions, it is difficult to experimentally assess Reynolds Number, pitching hull and splashing effects (as well as variations in Table 1 parameters) on use of traditional scaling parameters for transient fluid interaction problems. Since the NTT approach provides transient forces,

velocities, pressures and wave shapes for both model and full-scale hull, the differences in results, as dependent upon viscosity and turbulence parameters, can be determined. The comparison of results then can provide Froude and Reynolds number correlations that provide an improvement over traditional scaling laws.

In final summary then, the NTT methodology shows promise in its early stages of development for solving key problems in the steady-state and transient loading of off-shore structures. As free-surface computational techniques improve together with computational speed capability, NTT methodology will undoubtedly improve as a source of reliable and accurate load prediction in the years ahead to supplement standard test tank methods.

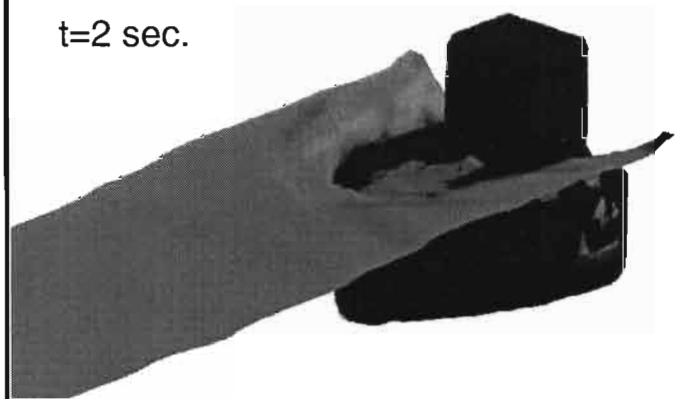
### References

1. Hirt, C. W., FLOW-3D Quick Reference Guide, Version 7.0, Flow Science, Inc., Los Alamos, New Mexico, 1995.
2. Hirt, C. W. and Nichols, B. D., Volume of Fluid (VOF) Method for the Dynamics of Free Boundaries, *J. Comp. Phys.* 39, Vol. 201, 1981.
3. Sicilian, J. M., and Hirt, C. W., HYDR-3D, A Solution Algorithm for Transient 3-D Flows, Flow Science, Inc., Los Alamos, NM, 1985.
4. Hirt, C. W., Amsdem, A. A. And Cook, J. L., An Arbitrary Lagrangian-Eulerian Computing Method for all Flow Speeds, *J. Comp. Phys.* 14, Vol. 227, 1974.
5. ANSYS Users' Manual, Swanson Analysis Systems, Inc., Revision 5.0, Houston, PA, 1992.
6. Buchner, B., The Impact of Green Water on FPSO Design, MARIN Report 255704-OP, Maritime Research Institute Netherlands, Wageningen, Netherlands, 1995 (also OTC Paper 7698, 1995).
7. Buchner, B., The Impact of Green Water Loading on Ship and Offshore Unit Design, MARIN Report 255704-OP, Maritime Research Institute Netherlands, Wageningen, Netherlands, 1995.
8. Wiegel, R. L., Oceanographic Engineering, Prentice-Hall, Englewood Cliffs, NJ, 1964.
9. Krauss, W., Dynamics of the Homogeneous and Quasihomogeneous Ocean, Vol. 1, Gebruder Borntraeger Publishers, Berlin, 1973.
10. Oil Companies International Marine Forum (OCIMF), Prediction of Wind and Current Loads on VLCC's, 2<sup>nd</sup> Edition, Witherby and Co., London, 1994.
11. Ortloff, C. R., FPSO Green Water Interaction and Load Prediction Methodology by Computational Fluid Dynamics Methods, FMC Corporate Technology Center Report 7024, Santa Clara, CA, September, 1995.
12. Wichers, J. E. W., A Simulation Model for a Single Point Moored Tanker, Maritime Research Institute Netherlands Report 797, Wageningen, Netherlands, June, 1988.



FPSO HULL ANSYS MODEL

Fig. 1



t=2 sec.

MODEL/PROTOTYPE SCALE 1:60

Fig. 4

FPSO HULL WAVE INTERACTION

t=0 sec.

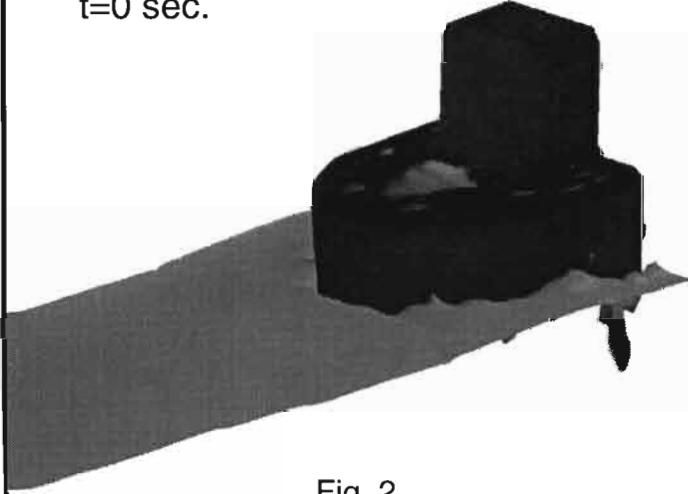


Fig. 2

t=2.5 sec.

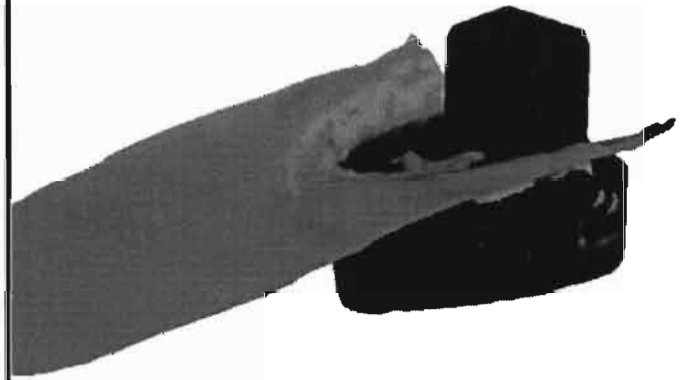


Fig. 5

t= 1.0 sec.

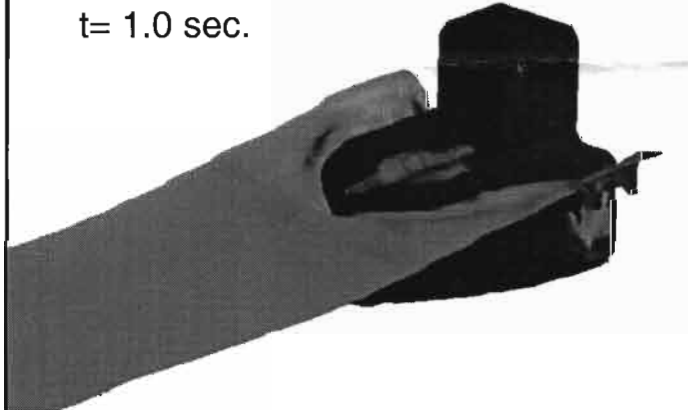


Fig. 3

t= 3.5 sec.

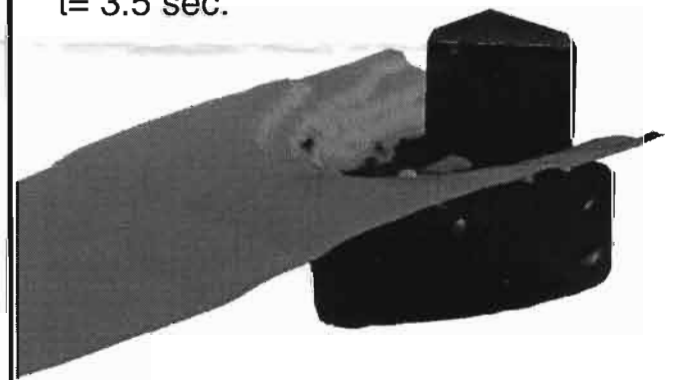


Fig. 6

t= 4.0 sec.

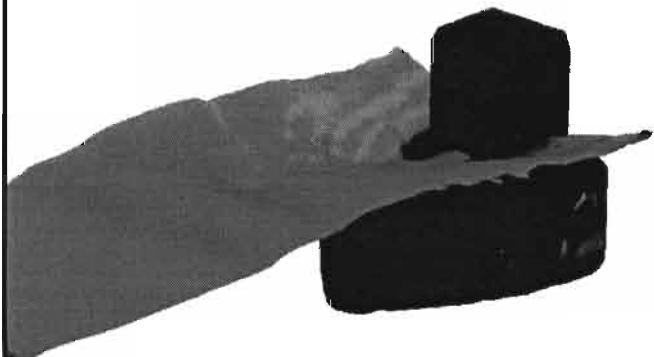


Fig. 7

t= 7 sec.

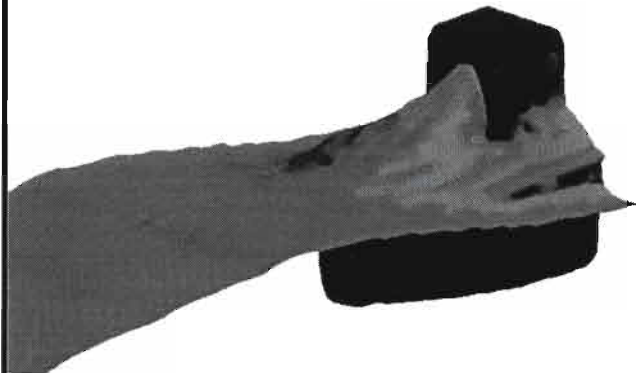


Fig. 10

t=4.5 sec.

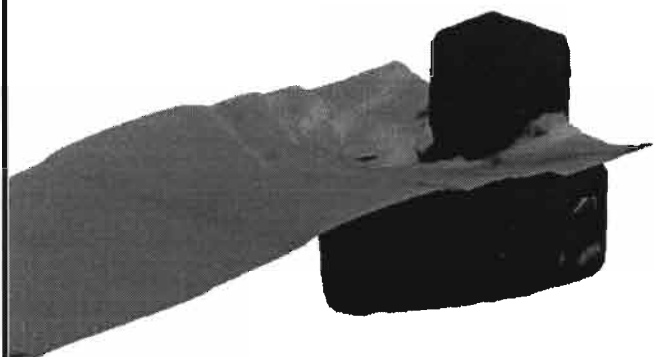


Fig. 8

t= 8.0 sec.

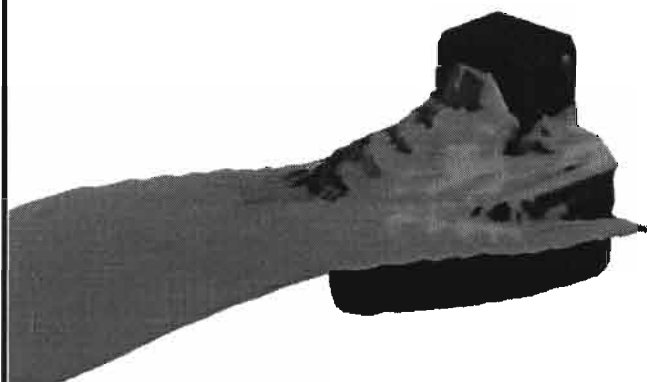


Fig. 11

t= 6.0 sec.

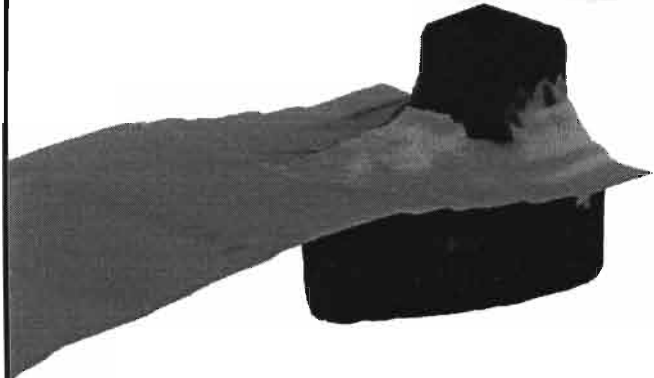


Fig. 9

t= 8.5 sec.

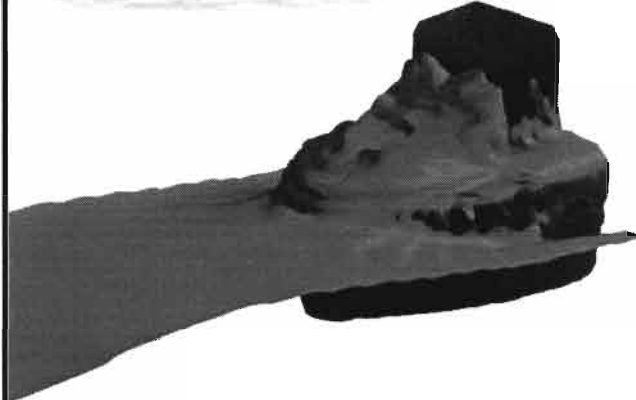


Fig. 12



t= 9.0 sec.

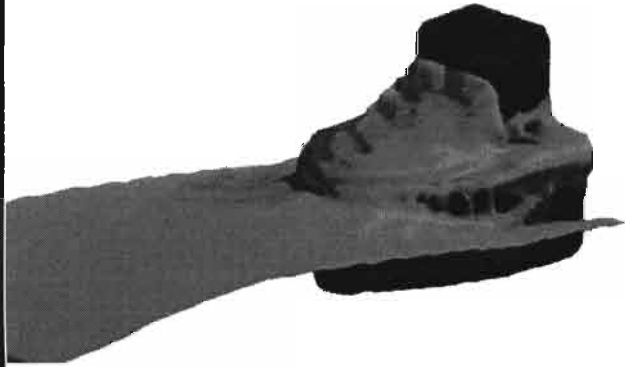


Fig. 13

t= 11 sec.

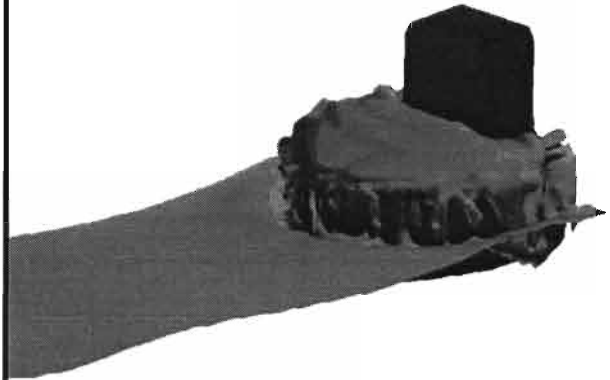


Fig. 16

t= 10.0 sec.

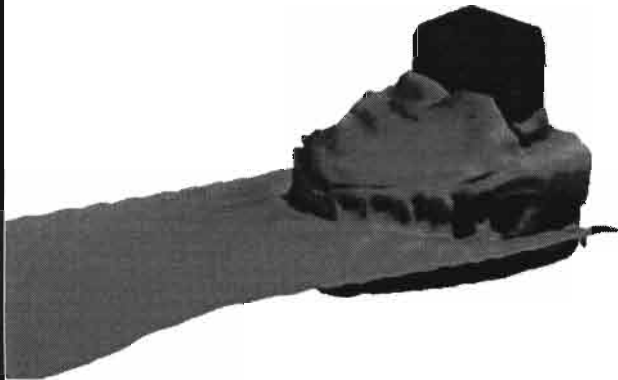


Fig. 14

t= 11.5 sec.

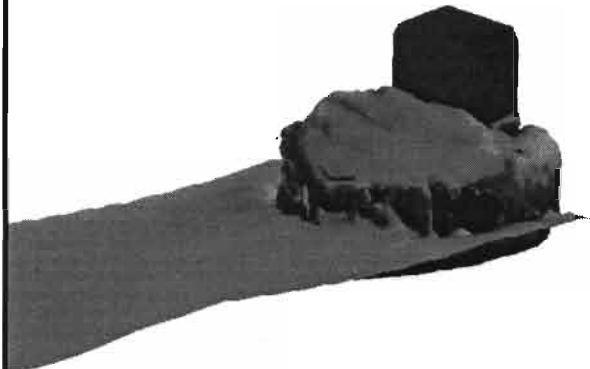


Fig. 17

t= 10.5 sec.

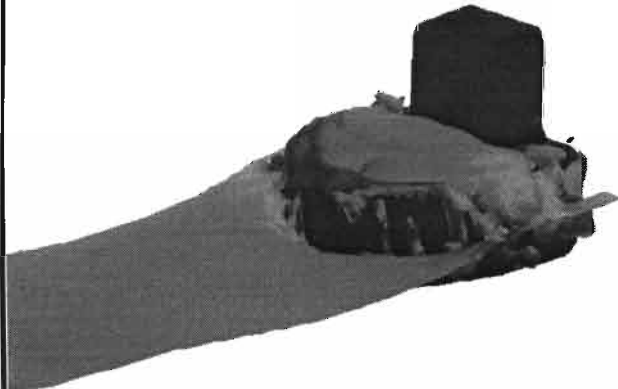


Fig. 15

t= 13 sec.

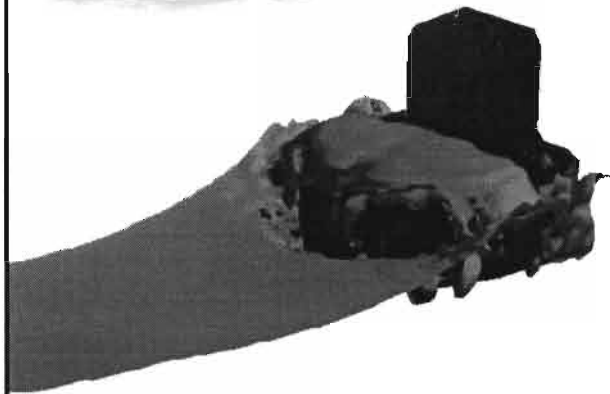


Fig. 18